Understanding laser stabilization using spectral hole burning

B. Julsgaard, A. Walther, S. Kröll, L. Rippe

Department of Physics, Lund Institute of Technology, P.O. Box 118, SE-22100 Lund, Sweden

bju@com.dtu.dk

Abstract: There have recently been several studies of the performance of laser frequency stabilization using spectral holes in solids, instead of an external cavity, as a frequency reference. Here an analytical theory for Pound-Drever-Hall laser frequency stabilization using spectral hole-burning is developed. The interaction between the atomic medium and the phase modulated light is described using a linearized model of the Maxwell-Bloch equations. The interplay between the carrier and modulation sidebands reveals significant differences from the case of locking to a cavity. These include a different optimum modulation index, an optimum sample absorption, and the possibility to lock the laser in an inherent linear frequency drift mode. Spectral holes in solids can be permanent or transient. For the materials normally used, the dynamics and time scales of transient holes often depend on population relaxation processes between ground state hyperfine levels. These relaxation rates can be very different for different solid state materials. We demonstrate, using radio-frequency pumping, that the hyperfine population dynamics may be controlled and tailored to give optimum frequency stabilization performance. In this way also materials with initially non-optimum performance can be used for stabilization. The theoretical predictions regarding the inherent linear frequency drift is compared to experimental data from a dye laser stabilized to a spectral hole in a Pr^{3+}:Y_2SiO_5 crystal.

OCIS codes: (270.3430) Laser theory; (140.3425) Laser stabilization; (140.2050) Dye lasers.

References and links

1. R. W. P. Drever, J. L. Hall, F. V. Kowalski, J. Hough, G. M. Ford, A. J. Munley, and H. Ward, "Laser phase and frequency stabilization using an optical resonator," Appl. Phys. B **31**, 97–105 (1983).
2. E. D. Black, "An introduction to Pound-Drever-Hall laser frequency stabilization," Am. J. Phys. **69**, 79–87 (2001).
3. P. B. Sellin, N. M. Strickland, J. L. Carlsten, and R. L. Cone, "Programmable frequency reference for subkilohertz laser stabilization by use of persistent spectral hole burning," Opt. Lett. **24**, 1038–1040 (1999).
4. N. M. Strickland, P. B. Sellin, Y. Sun, J. L. Carlsten, and R. L. Cone, "Laser frequency stabilization using regenerative spectral hole burning," Phys. Rev. B **62**, 1473–1476 (2000).
5. G. J. Pryde, T. Böttger, and R. L. Cone, "Numerical modeling of laser stabilization by regenerative spectral hole burning," J. Lumin. **94-95**, 587–591 (2001).
6. G. J. Pryde, T. Böttger, R. L. Cone, and R. C. C. Ward, "Semiconductor lasers stabilized to spectral holes in rare earth crystals to a part in 10(13) and their application to devices and spectroscopy," J. Lumin. **98**, 309–315 (2002).
7. P. B. Sellin, N. M. Strickland, T. Böttger, J. L. Carlsten, and R. L. Cone, "Laser stabilization at 1536 nm using regenerative spectral hole burning," Phys. Rev. B **63**, 155111 (2001).
8. T. Böttger, Y. Sun, G. J. Pryde, G. Reinemer, and R. L. Cone, "Diode laser frequency stabilization to transient spectral holes and spectral diffusion in Er^{3+}:Y_2SiO_5 at 1536 nm," J. Lumin. **94**, 565–568 (2001).

#83390 - $15.00 USD Received 25 May 2007; revised 17 Aug 2007; accepted 19 Aug 2007; published 24 Aug 2007

9. T. Böttger, G. J. Pryde, and R. L. Cone, "Programmable laser frequency stabilization at 1523 nm by use of persistent spectral hole burning," Opt. Lett. **28**, 200–202 (2003).
10. K. D. Merkel, R. D. Peters, P. B. Sellin, K. S. Repasky, and W. R. Babbitt, "Accumulated programming of a complex spectral grating," Opt. Lett. **25**, 1627–1629 (2000).
11. R. W. Equall, Y. Sun, R. L. Cone, and R. M. Macfarlane, "Ultraslow optical dephasing in Eu^{3+}:Y_2SiO_5," Phys. Rev. Lett. **72**, 2179–2181 (1994).
12. N. Ohlsson, R. K. Mohan, and S. Kröll, "Quantum computer hardware based on rare-earth-ion-doped inorganic crystals," Opt. Commun. **201**, 71–77 (2002).
13. I. Roos and K. Mølmer, "Quantum computing with an inhomogeneously broadened ensemble of ions: Suppression of errors from detuning variations by specially adapted pulses and coherent population trapping," Phys. Rev. A **69**, 022321 (2004).
14. J. J. Longdell and M. J. Sellars, "Experimental demonstration of quantum-state tomography and qubit-qubit interactions for rare-earth-metal-ion-based solid-state qubits," Phys. Rev. A **69**, 032307 (2004).
15. J. J. Longdell, M. J. Sellars, and N. B. Manson, "Demonstration of conditional quantum phase shift between ions in a solid," Phys. Rev. Lett. **93**, 130503 (2004).
16. J. H. Wesenberg, K. Mølmer, L. Rippe, and S. Kröll, "Scalable designs for quantum computing with rare-earth-ion-doped crystals," Phys. Rev. A **75**, 012304 (2007).
17. L. Rippe, B. Julsgaard, A. Walther, and S. Kröll, "Laser stabilization using spectral hole burning," http://arxiv.org/abs/quant-ph/0611056.
18. D. Allen and J. H. Eberly, *Optical resonance and two-level atoms* (Wiley, New York, 1975).
19. P. W. Milonni and J. H. Eberly, *Lasers* (John Wiley & Sons, New York, 1988).
20. L. Mandel and E. Wolf, *Optical Coherence and Quantum Optics* (Cambridge University Press, New York, 1995).
21. A. M. Stoneham, "Shapes of Inhomogeneously Broadened Resonance Lines in Solids," Rev. Mod. Phys. **41**, 82 (1969).
22. J. H. Wesenberg and K. Mølmer, "Field Inside a Random Distribution of Parallel Dipoles," Phys. Rev. Lett. **93**, 143903 (2004).
23. G. C. Bjorklund, M. D. Levenson, W. Lenth, and C. Ortiz, "Frequency modulation (FM) spectroscopy," Appl. Phys. B **32**, 145–152 (1983).
24. T. Böttger, G. J. Pryde, C. W. Thiel, and R. L. Cone, "Laser frequency stabilization at 1.5 microns using ultra-narrow inhomogeneous absorption profiles in Er^{3+}:$LiYF_4$," J. Lumin. **127**, 83–88 (2007).
25. L. Rippe, "Quantum computing with naturally trapped sub-nanometre-spaced ions," Ph.D. thesis, Division of Atomic Physics, LTH, P.O. Box 118, SE 221 00 Lund (2006).
26. "Laser stabilization system documentation," available at http://www.atom.fysik.lth.se/QI/.
27. K. J. Åström and R. J. Murray, "*Feedback Systems: An Introduction for Scientists and Engineers*," preprint at http://www.cds.caltech.edu/ murray/amwiki/.
28. F. Wolf, "Fast sweep experiments in microwave spectroscopy," J. Phys. D **27**, 1774–1780 (1994).
29. T. Chang, M. Z. Tian, R. K. Mohan, C. Renner, K. D. Merkel, and W. R. Babbitt, "Recovery of spectral features readout with frequency-chirped laser fields," Opt. Lett. **30**, 1129–1131 (2005).
30. M. Nilsson, L. Rippe, R. Klieber, D. Suter, and S. Kröll, "Holeburning techniques for isolation and study of individual hyperfine transitions in inhomogeneously broadened solids, demonstrated in Pr^{3+}:Y_2SiO_5," Phys. Rev. B **70**, 214116 (2004).
31. J. D. Jackson, *Classical Electrodynamics* (John Wiley & Sons, New York, 1988).

1. Introduction

Frequency stabilization of lasers is an advanced topic in the science of optical physics, and the use of optical cavities in the Pound-Drever-Hall scheme [1] is an often used technique, which is also theoretically very well understood [2]. Since the late 1990'ies, laser frequency stabilization using spectral hole burning has been developed using semi-conductor lasers [3, 4, 5, 6, 7, 8, 9] or a Ti:sapphire laser [10]. However, the theoretical understanding of this stabilization method is not well developed. Such a theory must include the interaction between the laser to be stabilized and the atomic reference material in which case the equations of motion are inherently non-linear. In this paper we present an analytical, linearized theory, which gives physical insight to the spectral hole burning dynamics and its implication on the frequency stabilization feedback loop. The theory gives optimum design parameters for the stabilization feedback system, and in particular we demonstrate that an inherent linear laser frequency drift can be avoided with certain parameter choices.

The inherent linear frequency drift regime is also identified experimentally with a dye laser

#83390 - $15.00 USD Received 25 May 2007; revised 17 Aug 2007; accepted 19 Aug 2007; published 24 Aug 2007

stabilized to the 606 nm transition in Pr^{3+}:Y_2SiO_5. In order to control the hole-burning dynamics in this material, we introduced an "RF-eraser", which consists of RF magnetic fields, allowing us to vary the hyperfine level lifetimes.

Optical cavities are widely used for laser stabilization, but in some cases the use of spectral holes can be advantageous. Firstly, if one wishes to perform experiments on optical transitions in the hole-burning material itself, it may be required that the phase coherence time of the laser is similar to the coherence time, T_2, of the optical transition. The hole-burning material itself is then automatically sufficient as a phase reference. For instance, the 580 nm transition in Eu^{3+}:Y_2SiO_5 has an optical coherence time as long as 2.6 ms [11]. Secondly, when using the spectral-hole-burning technique, the sensitivity to vibrations requires that the atomic medium moves much less than an optical wavelength in an optical coherence time. However, for the mirrors in a high-finesse cavity this sensitivity is essentially multiplied by the average number of round trips made by a photon in the cavity, which can be several orders of magnitude. In practice, the hole-burning materials require cryogenic cooling in which case vibration stability is more difficult than for an optical cavity. However, if it is possible to use the same hole-burning crystal for laser stabilization and for further experiments, the sensitivity to vibrations is reduced significantly, and much of the technology for the experiments can be re-used in the laser stabilization.

For transient spectral hole systems the long-term stability presents a challenge since the spectral hole position may change over time. Rare-earth-metal-doped crystals are interesting for, among others, implementing quantum information protocols [12, 13, 14, 15, 16].

In Sec. 2 the analytical theory of laser frequency stabilization using spectral hole burning is developed as the main result of this paper. After a brief description of the experimental setup in Sec. 3, we make an experimental study of the laser frequency drift dynamics in Sec. 4. The paper is concluded in Sec. 5.

2. Theoretical description of laser stabilization using spectral hole burning

It is our intention in this paper to maintain the physical understanding, and hence we will restrict ourselves to analytical derivations and make approximations, rather than numerical simulations, when the calculations become difficult. Our theory is quantitatively accurate for many practical systems. Below we derive in detail the basic model for the the laser stabilization. In Sec. 2.4 we give briefly the main ideas and results behind the model of inherent linear frequency drift. Additional details on the theory can be found in [17].

2.1. Two-level atoms and Maxwell-Bloch equations

We start with an ensemble of inhomogeneously broadened two-level atoms. We allow laser light to propagate through these along the z-direction. With a large beam cross section a one-dimensional theory is sufficient, and the Maxwell-Bloch equations can be written (see e.g. [18, 19, 20]):

$$\frac{\partial}{\partial t}(u-iv) = -(\frac{\Gamma_h}{2}+i\Delta)(u-iv) - i\Omega w, \tag{1}$$

$$\frac{\partial}{\partial t}w = \frac{i}{2}\left[\Omega(u+iv) - \Omega^*(u-iv)\right] - \frac{1}{T_1}(1+w), \tag{2}$$

$$\left(\frac{\partial}{\partial z} + \frac{n_b}{c}\frac{\partial}{\partial t}\right)\Omega = \frac{i\alpha_0}{2\pi}\int_{-\infty}^{\infty} g(\Delta)(u-iv)d\Delta. \tag{3}$$

Here (u,v,w) is the usual Bloch-vector which depends on time t, position z, and detuning Δ (from a chosen reference point). The electric field is described in terms of the complex Rabi frequency $\Omega(z,t) = \mu\mathscr{E}(z,t)/\hbar$, where $\mathscr{E}$ is the complex electric field and μ is the dipole moment

#83390 - $15.00 USD Received 25 May 2007; revised 17 Aug 2007; accepted 19 Aug 2007; published 24 Aug 2007

along the direction of the field (we consider only a single linear polarization mode). $\Gamma_h = 2/T_2$ is the FWHM homogeneous line-width of the atoms in rad/sec, T_1 and T_2 are the life and coherence times of the optical transition, respectively. In Eq. (3) n_b is the refractive index of non-absorbing background atoms, and $g(\Delta)$ is a dimensionless function describing the inhomogeneous distribution of atoms such that $g(\Delta)$ is proportional to the number of atoms with transition frequency Δ. We use an unconventional but experimentally convenient normalization such that $g(\Delta_0) = 1$ if α_0 is the absorption coefficient measured with a weak laser field at frequency Δ_0. The integral over Δ in Eq. (3) effectively adds the contribution of the polarization from all the atoms to the electric field Ω at position z and time t.

Eqs. (1-3) are in general difficult to solve analytically. However, for our specific needs regarding laser stabilization we will make a number of approximations in the following. We start by noting that in Eq. (3) the term $\frac{n_b}{c}\frac{\partial \Omega}{\partial t}$ is only relevant when describing very fast changes on the time scale L/c where L is the length of the sample, and it can be neglected here.

2.1.1. Linear regime of Maxwell-Bloch equations

The next approximation is to consider Eqs. (1-3) in the linear regime where, $w \approx -1$ for all atoms, i.e. the probability of being in the excited state is small. In Sec. 2.2 we discuss the validity of this approximation. Inserting (with $w = -1$) the integral form $u(z,t) - iv(z,t) = i\int_{-\infty}^{t} e^{-(\frac{\Gamma_h}{2}+i\Delta)(t-t')}\Omega(z,t')dt'$ of Eq. (1) into Eq. (3) and expressing the electric field Ω in terms of its Fourier components, $\Omega(z,t) = \int_{-\infty}^{\infty}\Omega(z,\omega)e^{-i\omega t}d\omega$, it follows that Eq. (3) can be written in Fourier space as:

$$\begin{aligned}\frac{\partial}{\partial z}\Omega(z,\omega) &= -\frac{\alpha_0}{2\pi}\int_{-\infty}^{\infty}\frac{g(\Delta)d\Delta}{\frac{\Gamma_h}{2}+i(\Delta-\omega)}\Omega(z,\omega)\\ &\equiv -\frac{\alpha_R(\omega)+i\alpha_I(\omega)}{2}\Omega(z,\omega).\end{aligned} \tag{4}$$

where we define $\alpha_R(\omega)$ and $\alpha_I(\omega)$ as the real and imaginary absorption coefficients, respectively. For a single frequency component of the field $\Omega(z,\omega) = A(z,\omega)e^{-i\phi(z,\omega)}$ with real amplitude A and phase ϕ we have the relation:

$$\frac{\partial A(z,\omega)}{\partial z} = -\frac{\alpha_R(\omega)}{2}A(z,\omega), \tag{5}$$

$$\frac{\partial \phi(z,\omega)}{\partial z} = +\frac{\alpha_I(\omega)}{2}. \tag{6}$$

Here α_R is the normal absorption coefficient, and α_I is related to the total index of refraction by $n(\omega) = n_b + \frac{\lambda\alpha_I(\omega)}{4\pi}$ with λ being the vacuum wavelength of the radiation. Eqs. (4-6) will be the workhorse for many calculations in the following sections. Our goal is to model the frequency variations of the incoming laser field, propagate this field through the atomic medium via Eqs. (5) and (6), and finally derive an error signal useful for frequency stabilization based on the outgoing field. We will reach this goal in Sec. 2.3, but before that we introduce a model which describes the effect of hole burning in terms of the shape function, $g(\Delta)$.

2.2. Two-level atoms with a reservoir state

The calculations in the previous sections need to be refined in order to describe the effect of spectral hole burning. So, in addition to the ground $|g\rangle$ and excited $|e\rangle$ states we add a third

#83390 - $15.00 USD Received 25 May 2007; revised 17 Aug 2007; accepted 19 Aug 2007; published 24 Aug 2007

reservoir state $|\mathrm{r}\rangle$ (see Fig. 4(b)) and write the Bloch equations for these:

$$\frac{\partial}{\partial t}(u-iv) = -(\frac{\Gamma_\mathrm{h}}{2}+i\Delta)(u-iv) - i\Omega(\rho_e-\rho_g), \tag{7}$$

$$\frac{\partial \rho_e}{\partial t} = \frac{i}{4}\left[\Omega(u+iv)-\Omega^*(u-iv)\right] - \frac{1}{T_1}\rho_e, \tag{8}$$

$$\frac{\partial \rho_g}{\partial t} = -\frac{i}{4}\left[\Omega(u+iv)-\Omega^*(u-iv)\right] + \frac{b_\mathrm{eg}}{T_1}\rho_e - \frac{1}{T_\mathrm{gr}}\rho_g + \frac{1}{T_\mathrm{rg}}\rho_r, \tag{9}$$

$$\frac{\partial \rho_r}{\partial t} = \frac{b_\mathrm{er}}{T_1}\rho_e + \frac{1}{T_\mathrm{gr}}\rho_g - \frac{1}{T_\mathrm{rg}}\rho_r. \tag{10}$$

We assume the optical field, Ω, only couples to the transition $|\mathrm{g}\rangle \rightarrow |\mathrm{e}\rangle$ and hence u and v still refer to this transition, and only the factor $w = \rho_\mathrm{e} - \rho_\mathrm{g}$ appears in the driving term in Eq. (7), as was the case in Eq. (1). We add the possibility of decays from the excited state to the reservoir state. The branching ratios from $|\mathrm{e}\rangle$ to $|\mathrm{g}\rangle$ and $|\mathrm{e}\rangle$ to $|\mathrm{r}\rangle$ are denoted b_eg and b_er, respectively. We also model relaxation between the $|\mathrm{g}\rangle$ and $|\mathrm{r}\rangle$ levels. The timescale for decays from $|\mathrm{g}\rangle$ to $|\mathrm{r}\rangle$ is T_gr, which in general need not be the same as the timescale T_rg in the opposite direction. For the homogeneous line-width, Γ_h, we now have $\frac{\Gamma_\mathrm{h}}{2} = \frac{1}{T_2} = \frac{1}{T_2^{(0)}} + \frac{1}{2T_\mathrm{gr}}$, where $T_2^{(0)}$ is the coherence time of the optical transition $|\mathrm{g}\rangle \rightarrow |\mathrm{e}\rangle$ in the absence of ground state relaxation, and the term $\frac{1}{2T_\mathrm{gr}}$ takes the finite lifetime of the state $|\mathrm{g}\rangle$ into account.

2.2.1. Separation of timescales

Our next step is to derive expressions, which characterize the shape of spectral holes burned by the laser field. From Eqs. (7-10) we compute the steady-state solutions for ρ_e, ρ_g, and ρ_r while u and v are still allowed to vary in time according to Eq. (7). This is a good approximation since in our specific case we have naturally different timescales for the ground state populations and the optical coherence, $T_\mathrm{rg}, T_\mathrm{gr} \gg T_2$. Furthermore, when the laser is actively stabilized to a line-width narrower than Γ_h, it is a good approximation to assume a zeroth order starting point, $\Omega = \Omega_0 e^{-i\Delta_0 t}$, where the laser is running perfectly at a monochromatic frequency, Δ_0. If the variations from this starting point are small, the populations will always be close to their steady-state values. With a little work we obtain and expression for the population difference $\rho_\mathrm{g} - \rho_\mathrm{e}$:

$$\rho_\mathrm{g} - \rho_\mathrm{e} = G\left(1 - d_\mathrm{hole}\frac{\frac{\Gamma_\mathrm{hole}^2}{4}}{\frac{\Gamma_\mathrm{hole}^2}{4} + (\Delta-\Delta_0)^2}\right), \tag{11}$$

where d_hole is the relative hole depth and Γ_hole is the FWHM of the hole. These parameters can be written:

$$d_\mathrm{hole} = \frac{(1+R)\frac{s_0}{2}}{1+(1+R)\frac{s_0}{2}}, \quad \Gamma_\mathrm{hole} = \Gamma_\mathrm{h}\sqrt{1+(1+R)\frac{s_0}{2}}, \tag{12}$$

where s_0 is the resonant saturation parameter:

$$s_0 = |\Omega_0|^2 T_1 T_2, \tag{13}$$

and for our particular case of Eqs. (7-10) we have:

$$R = \frac{1+\frac{b_\mathrm{er}T_\mathrm{rg}}{T_1}}{1+\frac{T_\mathrm{rg}}{T_\mathrm{gr}}}, \quad G = \frac{1}{1+\frac{T_\mathrm{rg}}{T_\mathrm{gr}}}. \tag{14}$$

#83390 - $15.00 USD Received 25 May 2007; revised 17 Aug 2007; accepted 19 Aug 2007; published 24 Aug 2007

The saturation parameter s_0 is a measure of the probability of an atom being in the excited state $|\mathrm{e}\rangle$ at resonance. In steady state at $\Delta = \Delta_0$ we have $\frac{\rho_\mathrm{e}}{\rho_\mathrm{g}} = \frac{s_0}{2} / \left(1 + \frac{s_0}{2}\right)$. The parameter G is a measure of the fraction of atoms in the ground state $|\mathrm{g}\rangle$ in equilibrium in the absence of the laser light or when the detuning, $\Delta - \Delta_0$, is large. The parameter R is a measure of how likely it is for an atom to be trapped in the reservoir state. The essence of R is in the term $b_\mathrm{er} T_\mathrm{rg}/T_1$, which is the ratio of the rate b_er/T_1 from $|\mathrm{e}\rangle$ into the reservoir state $|\mathrm{r}\rangle$ and the rate $1/T_\mathrm{rg}$ out of the reservoir state. From Eq. (12) it is clear that a spectral hole can be deep and broad for different reasons: Firstly, if the laser field is strong with a high saturation parameter s_0, although R is small, and secondly, if the trapping parameter R is large even a weak field with $s_0 \ll 1$ is capable of digging a deep, wide hole.

Now, we wish to employ Eq. (3) or (4) together with Eqs. (7-10). We insert the steady-state value of Eq. (11) into Eq. (7) written in integral form. Since the steady-state value is time-independent we may perform the same steps as those leading to Eq. (4). We will incorporate the value of $\rho_\mathrm{g} - \rho_\mathrm{e}$ into the $g(\Delta)$ shape function and just pretend that we never left the linear approximation, Eq. (4), of a two-level system. This is done correctly when:

$$g(\Delta) = \frac{\rho_\mathrm{g} - \rho_\mathrm{e}}{G} = 1 - \frac{d_\mathrm{hole} \frac{\Gamma_\mathrm{hole}^2}{4}}{\frac{\Gamma_\mathrm{hole}^2}{4} + (\Delta - \Delta_0)^2}. \tag{15}$$

The division by G (the fraction of atoms in $|\mathrm{g}\rangle$ far off resonance) assures that $g(\Delta)$ is correctly normalized to unity away from the spectral hole, i.e. α_0 is the absorption coefficient for a weak laser field in the absence of the spectral hole.

Let us retrace our steps so far and underline the approximations made. We have reached the two important equations (4) and (15). The $g(\Delta)$ function for a spectral hole describes how many atoms actually participate in the active two-level transition $|\mathrm{g}\rangle \rightarrow |\mathrm{e}\rangle$. We included the effect of saturation where atoms can also populate the excited state $|\mathrm{e}\rangle$ (which mathematically also creates a hole in $\rho_\mathrm{g} - \rho_\mathrm{e}$). However, since we assumed the populations ρ_e, ρ_g, and ρ_r to be essentially constant in time, we have restricted ourselves to solutions where the laser field does not deviate much from a perfect field, $\Omega = \Omega_0 e^{-i\Delta_0 t}$ (we have linearized the theory around this zeroth order solution). Note, that the field Ω can still have fast variations in e.g. its phase, as long as the phase excursions are not too large. Since both population trapping in the reservoir state and the effect of saturation (leading to population trapping in the excited state) are incorporated into the single parameter $g(\Delta)$, we effectively model the three-level equations (7-10) with our initial linear two-level system with low saturation, as described by Eq. (4).

Using Eq. (15) also requires another approximation. We note that d_hole and Γ_hole depend on the resonant saturation parameter, s_0. If the optical depth, $\alpha_0 L$, of the atomic sample is large, the saturation parameter will depend on z, and the use of a z-independent $g(\Delta)$ will be incorrect. However, if the laser field burns holes, the attenuation will be less than $\alpha_0 L$. Practically, the equations will be applicable for $\alpha_0 L$ not too much greater than unity.

Finally, we point out that d_hole and Γ_hole, as defined in Eq. (12), refer to the structure in the population, not to the depth and width which would be measured in an absorption experiment. From (12) we always have the relation:

$$1 - d_\mathrm{hole} = \left(\frac{\Gamma_\mathrm{h}}{\Gamma_\mathrm{hole}}\right)^2. \tag{16}$$

#83390 - $15.00 USD Received 25 May 2007; revised 17 Aug 2007; accepted 19 Aug 2007; published 24 Aug 2007

2.2.2. Absorption and phase shift from a spectral hole

Let us now employ Eqs. (4) and (15) to calculate the attenuation and phase shift of a laser field in the presence of a spectral hole. We take for the $g(\Delta)$ function:

$$g(\Delta) = \frac{\frac{\Gamma_{\text{inh}}^2}{4}}{\frac{\Gamma_{\text{inh}}^2}{4}+\Delta^2}\left(1 - \frac{d_{\text{hole}}\frac{\Gamma_{\text{hole}}^2}{4}}{\frac{\Gamma_{\text{hole}}^2}{4}+(\Delta-\Delta_0)^2}\right), \tag{17}$$

i.e. we have a spectral hole burned at frequency Δ_0 into an inhomogeneously broadened Lorentzian profile with width Γ_{inh} centered at $\Delta = 0$. Inserting this into Eq. (4) we find:

$$\frac{\alpha_{\text{R}}(\omega)}{\alpha_0} = \frac{\frac{\Gamma_{\text{inh}}^2}{4}}{\frac{\Gamma_{\text{inh}}^2}{4}+\omega^2} - \frac{\frac{\Gamma_{\text{inh}}^2}{4}}{\frac{\Gamma_{\text{inh}}^2}{4}+\Delta_0^2}\cdot\frac{\frac{\Gamma_{\text{hole}}(\Gamma_{\text{hole}}+\Gamma_{\text{h}})}{4}d_{\text{hole}}}{\frac{(\Gamma_{\text{hole}}+\Gamma_{\text{h}})^2}{4}+(\Delta_0-\omega)^2} \rightarrow 1 - \frac{\frac{\Gamma_{\text{hole}}(\Gamma_{\text{hole}}+\Gamma_{\text{h}})}{4}d_{\text{hole}}}{\frac{(\Gamma_{\text{hole}}+\Gamma_{\text{h}})^2}{4}+(\Delta_0-\omega)^2}, \tag{18}$$

$$\frac{\alpha_{\text{I}}(\omega)}{\alpha_0} = \frac{\omega\frac{\Gamma_{\text{inh}}}{2}}{\frac{\Gamma_{\text{inh}}^2}{4}+\omega^2} + \frac{\frac{\Gamma_{\text{inh}}^2}{4}}{\frac{\Gamma_{\text{inh}}^2}{4}+\Delta_0^2}\cdot\frac{\frac{\Gamma_{\text{hole}}}{2}(\Delta_0-\omega)d_{\text{hole}}}{\frac{(\Gamma_{\text{hole}}+\Gamma_{\text{h}})^2}{4}+(\Delta_0-\omega)^2} \rightarrow \frac{\frac{\Gamma_{\text{hole}}}{2}(\Delta_0-\omega)d_{\text{hole}}}{\frac{(\Gamma_{\text{hole}}+\Gamma_{\text{h}})^2}{4}+(\Delta_0-\omega)^2}, \tag{19}$$

with Γ_{hole} and d_{hole} defined in Eq. (12). In the first terms we assumed that $\Gamma_{\text{inh}} \gg \Gamma_{\text{h}}$. The arrows indicate the limit when $\Gamma_{\text{inh}} \rightarrow \infty$, i.e. when we neglect the effect of the possibly very wide inhomogeneous background. In case of a Gaussian inhomogeneous profile, the absorption and dispersion factors containing Γ_{inh} must be replaced by $\text{Re}\{w(Z)\}$ and $\text{Im}\{w(Z)\}$ with $Z = \frac{2\sqrt{\ln 2}}{\Gamma_{\text{inh}}}(\omega + i\frac{\Gamma_{\text{h}}}{2})$ known as the Voigt profile [19]. In general, the shape of the inhomogeneous profile varies depending on the broadening mechanism [21, 22].

If we compare Eqs. (15) and (18) we see that in an absorption measurement with a weak field (not changing the populations further) the measured width and depth of the hole are related to Γ_{hole} and d_{hole} by:

$$\Gamma_{\text{hole}}^{(\text{meas})} = \Gamma_{\text{hole}} + \Gamma_{\text{h}}, \quad d_{\text{hole}}^{(\text{meas})} = \frac{\Gamma_{\text{hole}} d_{\text{hole}}}{\Gamma_{\text{hole}} + \Gamma_{\text{h}}}. \tag{20}$$

2.3. Calculation of error signals

Now, let us turn to the calculation of real error signals used in the locking procedure. In reality the input light will vary in amplitude and frequency over time. Experimentally, the amplitude variations are easy to measure directly and and correct for. Hence, in the following we concentrate solely on frequency errors. A convenient method is to assume the incoming laser field to be of the form $\Omega(0,t) = \Omega_0 e^{-i(\Delta_0 t + \varepsilon\sin(\omega t))}$ i.e. we have an almost single-frequency laser at Δ_0, but with an additional small harmonic disturbance of the phase with frequency ω and magnitude ε, which we assume to be much less than unity. The complex Rabi frequency Ω_0 is given by $\Omega_0 = \frac{\mu}{\hbar}\sqrt{\frac{2\mu_0 cP}{n_{\text{b}}A}}$ where μ is the electrical dipole moment, μ_0 the vacuum permeability, c the speed of light, P the optical power, $\hbar$ Planck's constant divided by 2π, n_{b} the background refractive index of the atomic sample, and A the beam cross-sectional area. This model is valid when the laser is running in the frequency stabilized mode with a narrow line-width. When errors are small, the different frequency components will add linearly, and it is sufficient to consider a particular frequency ω.

In order to employ the Pound-Drever-Hall method, we phase modulate the laser beam at frequency, ω_{m}, with modulation index, m, leading to spectral hole burning at the laser base frequency, Δ_0, and at the sidebands $\Delta_0 \pm \omega_{\text{m}}$. Assuming $\Gamma_{\text{inh}} \gg \omega_{\text{m}}$, the two sideband spectral holes become identical, and taking $\varepsilon \ll 1$ we neglect hole burning effects from the ω-sidebands.

#83390 - $15.00 USD Received 25 May 2007; revised 17 Aug 2007; accepted 19 Aug 2007; published 24 Aug 2007

We describe the absorption and dispersion from the spectral holes by the transmission coefficients, η_i and phase shifts, ϕ_i, where $i = \mathrm{c,s}$ refer to "carrier" and "sideband", respectively:

$$\eta_i(\omega) = \exp\left(-\frac{\alpha_0 L}{2}\left[1 - \frac{\frac{\Gamma_{\mathrm{hole},i}(\Gamma_{\mathrm{hole},i}+\Gamma_\mathrm{h})}{4} d_{\mathrm{hole},i}}{\frac{(\Gamma_{\mathrm{hole},i}+\Gamma_\mathrm{h})^2}{4} + \omega^2}\right]\right), \tag{21}$$

$$\phi_i(\omega) = -\frac{\alpha_0 L}{2} \frac{\frac{\Gamma_{\mathrm{hole},i}}{2} d_{\mathrm{hole},i}\omega}{\frac{(\Gamma_{\mathrm{hole},i}+\Gamma_\mathrm{h})^2}{4} + \omega^2}, \tag{22}$$

We let the modulated field pass the atomic sample and collect it on a photo-detector. The detected power has a term oscillating at frequency ω_m given by:

$$\begin{aligned} P^{(\mathrm{out})}_{\omega_\mathrm{m}}(t) &= 4P^{(\mathrm{in})} J_0 J_1 \mathrm{Re}\left\{T(\omega)\cdot \varepsilon\omega e^{i\omega t}\right\} \cdot \sin(\omega_\mathrm{m} t), \\ T(\omega) &= \frac{\eta_\mathrm{c}(\omega)\eta_\mathrm{s}(0)e^{i\phi_\mathrm{c}(\omega)} - \eta_\mathrm{c}(0)\eta_\mathrm{s}(\omega)e^{i\phi_\mathrm{s}(\omega)}}{i\omega + \frac{1}{T_\mathrm{rg}}}. \end{aligned} \tag{23}$$

Here J_0 and J_1 are Bessel functions corresponding to the modulation index, m, and $P^{(\mathrm{in})}$ is the total incoming power. In the curly brackets the real part of the factor $\varepsilon\omega e^{i\omega t}$ is just the instantaneous frequency of the incoming laser (relative to Δ_0). Hence, the factor, $T(\omega)$, acts as a *transfer function* mapping this harmonic frequency excursion onto the measured power. This is similar to the way in which a complex impedance $Z(\omega)$ maps a complex current $I(\omega)$ onto a complex voltage $V(\omega) = Z(\omega)I(\omega)$ for individual Fourier components in electrical engineering. Hence, the transfer function, $T(\omega)$, is directly applicable for purposes of feedback loop design for the laser stabilization system.

In the denominator of $T(\omega)$, the term $\frac{1}{T_\mathrm{rg}}$ is added in order to compensate for the fact that $g(\Delta)$ is not time-independent on timescales slow compared to T_rg - the spectral holes are not permanent. This term arises from an ad hoc model, where the center frequency of the spectral hole, Δ_0, is varied as the instantaneous laser frequency, $\omega^{\mathrm{inst}} = \Delta_0 + \varepsilon\omega\cos(\omega t)$, weighted exponentially back in time with time constant, T_rg [17].

Eq. (23) is a very useful model for the atomic response to harmonic errors in laser frequency on all timescales. The transfer function $T(\omega)$ is important in the understanding of the interplay between the carrier and sideband holes. However, the extra ad hoc term $\frac{1}{T_\mathrm{rg}}$ in the denominator is far from giving the full picture of laser stability at low frequencies. This is discussed further in Sec. 2.4.

2.3.1. Evaluating the transfer function

The transfer function in Eq. (23) can be evaluated by using the expressions in Eqs. (21) and (22). When $\omega \ll \Gamma_{\mathrm{hole},i}$ we obtain:

$$T(\omega) \approx -\frac{\alpha_0 L}{\Gamma_\mathrm{h}} \frac{i\omega T_\mathrm{rg}}{1 + i\omega T_\mathrm{rg}} e^{-\frac{\alpha_0 L}{2}\left(\frac{1}{x_\mathrm{c}} + \frac{1}{x_\mathrm{s}}\right)} [f(x_\mathrm{c}) - f(x_\mathrm{s})]. \tag{24}$$

where the function f (shown in Fig. 1) is defined by:

$$f(x) = \frac{x-1}{x(x+1)}, \quad x_\mathrm{c} = \frac{\Gamma_{\mathrm{hole,c}}}{\Gamma_\mathrm{h}}, \quad x_\mathrm{s} = \frac{\Gamma_{\mathrm{hole,s}}}{\Gamma_\mathrm{h}}. \tag{25}$$

#83390 - $15.00 USD Received 25 May 2007; revised 17 Aug 2007; accepted 19 Aug 2007; published 24 Aug 2007

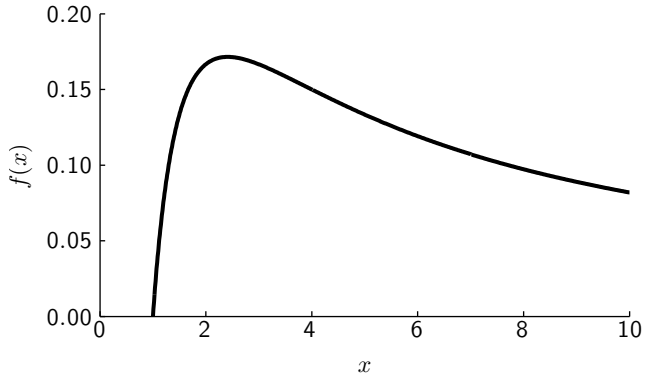

Fig. 1. The function $f(x)$ defined in Eq. (25). At $x = 2.41$ it attains its maximum value of 0.172. Physically, $f(x)$ is proportional to the slope of $\phi_i(\omega)$ at $\omega = 0$ in Eq. (22).

In the central regime, $T_{\mathrm{rg}}^{-1} \ll \omega \ll \Gamma_{\mathrm{hole},i}$, the term $\frac{i\omega T_{\mathrm{rg}}}{1+i\omega T_{\mathrm{rg}}}$ is unity and the transfer function is real. In the low-frequency limit, $\omega \ll T_{\mathrm{rg}}^{-1}$, the transfer function becomes imaginary and proportional to ω. In the high-frequency limit, $\omega \gg \Gamma_{\mathrm{hole}}$, we find:

$$T(\omega) \approx -\frac{1}{i\omega} e^{-\frac{\alpha_0 L}{2}} [e^{-\frac{\alpha_0 L}{2x_{\mathrm{c}}}} - e^{-\frac{\alpha_0 L}{2x_{\mathrm{s}}}}]. \tag{26}$$

The transfer function $T(\omega)$ has been plotted in Fig. 2 for a choice of reasonable experimental parameters. It is clear that there are three distinct regimes, as discussed above. Assuming that the terms in the square brackets in Eqs. (24) and (26) are positive, the transfer function is a negative real number times $i\omega$, 1, and $\frac{1}{i\omega}$ for the low-, medium-, and high-frequency regimes, respectively. This behavior is clearly seen in the magnitude of $T(\omega)$ shown on the upper plot in Fig. 2. The fact that the transfer function is real at medium frequencies means that the error signal $\propto \mathrm{Re}\{T(\omega)e^{i\omega t}\}$ will oscillate in phase with the actual frequency error $\propto \mathrm{Re}\{e^{i\omega t}\}$. For high frequencies, the extra $\frac{1}{i}$ factor makes the error signal oscillate as $\mathrm{Re}\{e^{i[\omega t-\pi/2]}\}$, i.e. the response is 90° delayed. This is shown as the phase reaching -90° in the lower plot in Fig. 2. For low frequencies the situation is the opposite; the phase is advanced by 90°. This behavior of the gain and phase has been previously reported in experiments and numerical simulations [5, 6].

In our calculations we always assume that the power in the carrier beam is higher than in either of the sidebands, leading to $\Gamma_{\mathrm{hole,c}} > \Gamma_{\mathrm{hole,s}}$. Then, according to the definition in Eq. (25), x_{c} will be larger than x_{s}, and the term in the square brackets in Eq. (26) will be positive, as we assumed above. For Eq. (24), however, we can have a situation where $f(x_{\mathrm{c}}) < f(x_{\mathrm{s}})$ if, e.g. $2.41 < x_{\mathrm{s}} < x_{\mathrm{c}}$, according to Fig. 1. In this case there is a 270° phase shift between the medium- and high-frequency regimes which in practice means that the sign of the error signal cannot be chosen correctly for all frequency components in a closed feedback loop. Physically, the sign change occurs when the slope of $\phi_{\mathrm{c}}(\omega)$ around $\omega = 0$ equals the slope of $\phi_{\mathrm{s}}(\omega)$ in Eq. (22) and we must assure that this is never the case. Note also that prior to and in the initialization of the laser locking feedback loop the spectral holes are broad and shallow (since the laser is broadband). The carrier hole will be deeper than the sideband holes while the widths are roughly the same, limited by the broad laser line-width. This in turn assures that the slope of $\phi(\omega)$ for the carrier is larger than for the sidebands. We must choose the right parameters such that the sign will remain correct when the feedback loop is closed and the laser line width

#83390 - $15.00 USD Received 25 May 2007; revised 17 Aug 2007; accepted 19 Aug 2007; published 24 Aug 2007

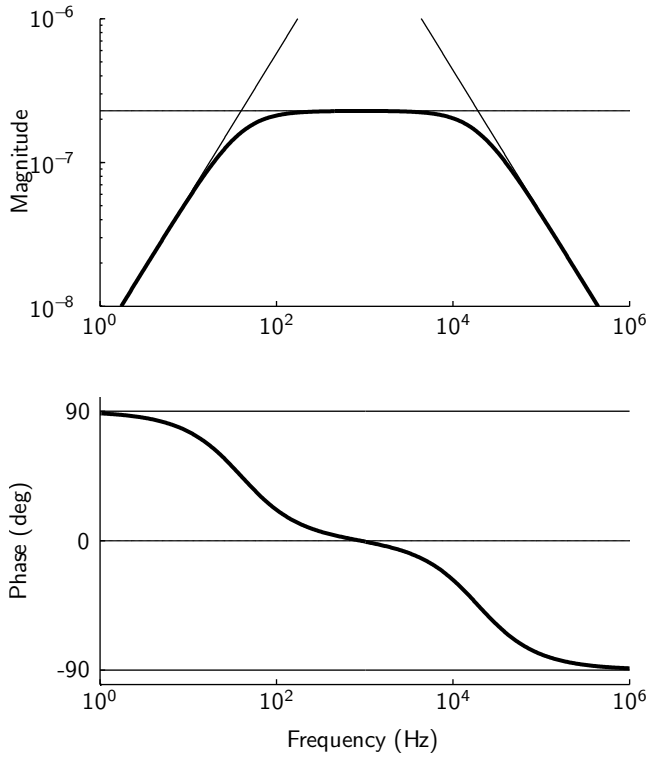

Fig. 2. The magnitude and phase of the transfer function $T(\omega)$ calculated from Eq. (23) (heavy lines). The light lines show the asymptotic cases discussed around Eqs. (24) and (26). Parameters used are $T_1 = 150$ µs, $T_2 = 18$ µs, $T_{\mathrm{rg}} = T_{\mathrm{gr}} = 4$ ms, $b_{\mathrm{er}} = 0.5$, $\Omega_0 = 2\pi \cdot 1$ kHz, and $m = 0.40$, giving $\Gamma_{\mathrm{h}} = 2\pi \cdot 17.5$ kHz, $\Gamma_{\mathrm{hole,c}} \approx 2\pi \cdot 21$ kHz and $\Gamma_{\mathrm{hole,s}} \approx 2\pi \cdot 18$ kHz. These parameters are close to our experimental working values, as we shall see in Sec. 4.

narrows.

2.3.2. Parameter choices for obtaining a large error signal

The theoretical observations above enable us to discuss the optimum parameters in general. A few design considerations are also given in connection with our particular experimental setup, see Sec. 3.

In order to obtain a large error signal, our first observation is the fact that the detected power given in Eq. (23) is proportional to $P^{(\mathrm{in})}$. It is no surprise that more light gives a higher signal at the detector, but it is wrong to just naively increase the incoming light power $P^{(\mathrm{in})}$ and expect a better performance. Doing so will increase s_0 in Eq. (13) and in turn the hole widths $\Gamma_{\mathrm{hole},i}$ in Eq. (12). However, increasing the incoming power and at the same time increasing the beam area, A, leading to an unchanged intensity, will always help. Hence, it is a good idea to use an atomic sample with a large area.

Next we observe in Eq. (23) that the front factor $J_0 J_1$ attains its maximum value of 0.339 when the modulation index is $m = 1.08$. This value is often used in laser stabilization setups utilizing optical cavities [2]. However, as opposed to the resonance lines in a cavity, the shape of spectral holes depends on the optical power. If the carrier and sideband powers were equal the holes would be identical, i.e. $\eta_{\mathrm{c}} = \eta_{\mathrm{s}}$ and $\phi_{\mathrm{c}} = \phi_{\mathrm{s}}$, leading to a zero error signal according

#83390 - $15.00 USD Received 25 May 2007; revised 17 Aug 2007; accepted 19 Aug 2007; published 24 Aug 2007

to Eq. (23). For this reason the optimum modulation index is lower than 1.08, leading to a more asymmetric power distribution between the carrier and the sidebands. We have searched our parameter space with numerical methods while optimizing the signal in Eq. (23). The result is that $m = 0.56$ is a good choice. However, there are further complications regarding the laser stability which suggest that m should be even lower. This will be discussed in Sec. 2.4.

Regarding the hole widths $\Gamma_{\mathrm{hole,c}}$ and $\Gamma_{\mathrm{hole,s}}$ it is clear from Eq. (24) and Fig. 1 that $x_{\mathrm{c}} = \Gamma_{\mathrm{hole,c}}/\Gamma_{\mathrm{h}}$ should not be much greater than 2.41, since a higher value simply makes the f-function decrease again. Also, we would like to make $x_{\mathrm{s}} = \Gamma_{\mathrm{hole,s}}/\Gamma_{\mathrm{h}}$ small in order to decrease $f(x_{\mathrm{s}})$. We can do this by lowering the modulation index m. Making m too small will also lower the factor $J_0 J_1$ and this is why we found $m = 0.56$ to be the optimum choice seen solely from the point of view of optimizing the error signal. However, the magnitude of the error signal is not everything. The narrower the hole widths $\Gamma_{\mathrm{hole},i}$, the longer the duration of the atomic phase memory and hence potentially better phase stability of the laser can be obtained. We should also note that a given width, $\Gamma_{\mathrm{hole},i}$, can be obtained in different ways according to Eq. (12). One could choose a high intensity (high s_0) and a short hole lifetime T_{rg} (low R according to (14)) if adjustable. On the other hand, a low intensity and a long hole lifetime could give the same result. In general, the latter will give the better long-term stability of the spectral hole.

To estimate the optimum optical density $\alpha_0 L$ let us assume that $x_{\mathrm{c}} \approx 2$ and $x_{\mathrm{s}} \approx 1$. This is not far from optimum given the discussion above. Inserting this into either Eq. (24) or (26) leads to the ballpark estimate $\alpha_0 L \approx 1.15$, corresponding to a background intensity transmission of $e^{-\alpha_0 L} \approx 32\%$. Note, this is on the edge of our approximation that $\alpha_0 L$ should not be too large for quantitatively correct results.

2.4. Laser drift

In the previous sections we have calculated the error signals for laser locking based on the linearized model with the time-independent distribution function $g(\Delta)$. For slowly varying errors on timescales slower than the hole lifetime, T_{rg}, we presented in connection with Eq. (23) an ad hoc model to describe the dynamics when $\omega \to 0$. However, this does not really illustrate the real challenges in long-term stability of the laser frequency. First of all, note that $T(\omega) \to 0$ when $\omega \to 0$, which is a consequence of the fact that a transient spectral hole is not a fixed frequency reference. This means that on long timescales the laser frequency stability will depend highly on e.g. measurement noise and offset tolerances in the electronic system.

We discuss in the present section that, in addition to these problems, under certain conditions there is a solution to the equations where the laser is locked, but the frequency is drifting linearly with time. Below we will re-calculate the absorption coefficients α_{R} and α_{I} in the presence of laser drift, which leads to corrections to the error signal.

2.4.1. The drift model

We consider a situation where the incoming laser field is given by $\Omega(0,t) = \Omega_0 e^{-i(\Delta_0 + \frac{\beta t}{2})t}$ corresponding to an instantaneous linear frequency variation, $\omega_{\mathrm{inst}} = \Delta_0 + \beta t$, where β is the drift rate in rad/s^2. This ansatz leads to a time-dependent version of Eqs. (7-10), which can be solved by numerical methods. However, our aim is to derive an intuitive condition for the presence of a linear laser drift, which can be done analytically in perturbation theory by making a series expansion of ρ_{e}, ρ_{g}, and ρ_{r} in the dimensionless parameter $\xi = \frac{\beta T_{\mathrm{rg}}}{\Gamma_{\mathrm{hole}}}$. This parameter is a measure of how far the laser drifts during a hole lifetime, T_{rg}, compared to the width of the hole, Γ_{hole}.

By expanding $\rho_{\mathrm{e}} = \rho_{\mathrm{e}}^{(0)} + \xi \rho_{\mathrm{e}}^{(1)} + \xi^2 \rho_{\mathrm{e}}^{(2)} + \ldots$, and similarly for ρ_{g} and ρ_{r}, we may calculate the corresponding distribution function $g(\Delta) = \frac{1}{G}(\rho_{\mathrm{g}} - \rho_{\mathrm{e}}) = \frac{1}{G}(\rho_{\mathrm{g}}^{(0)} - \rho_{\mathrm{e}}^{(0)}) + \frac{\xi}{G}(\rho_{\mathrm{g}}^{(1)} - \rho_{\mathrm{e}}^{(1)}) + O(\xi^2)$. The term linear in ξ is our correction, $g_{\mathrm{drift}}(\Delta)$, to the shape function $g(\Delta)$ due to the

#83390 - $15.00 USD Received 25 May 2007; revised 17 Aug 2007; accepted 19 Aug 2007; published 24 Aug 2007

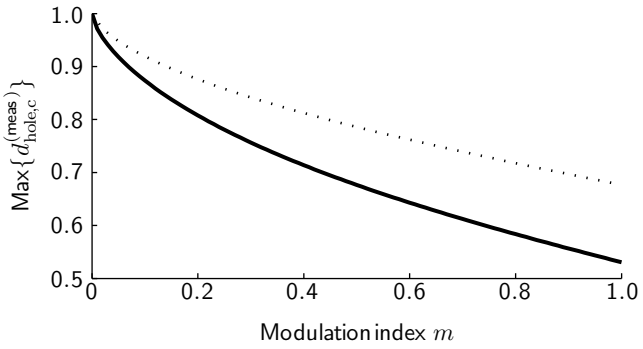

Fig. 3. Thresholds for stable laser operation. If $d_{\mathrm{hole,c}}^{(\mathrm{meas})}$ is below the solid line the square bracket in Eq. (28) is positive and the zero-drift solution is stable. In order for the low-frequency part of the laser locking to have the correct sign ($f(x_{\mathrm{c}}) - f(x_{\mathrm{s}}) > 0$ in Eq. (24)) we require the less stringent condition that $d_{\mathrm{hole,c}}^{(\mathrm{meas})}$ is below the dotted line. Between the two lines the laser can be locked in a linearly drifting mode.

drift. By inserting $g_{\mathrm{drift}}(\Delta)$ into Eq. (4) and evaluating the result at $\omega = \Delta_0$, we calculate the imaginary absorption coefficient α_{I} experienced by the laser beam at frequency Δ_0 drifting at rate β. The calculations are quite cumbersome [17], we just present the result:

$$\alpha_{\mathrm{I}}(\Delta_0) = -\alpha_0 \left(\frac{\beta T_{\mathrm{rg}}}{\Gamma_{\mathrm{hole}}}\right) d_{\mathrm{hole}} \times \frac{\frac{T_1}{T_{\mathrm{rg}}}\left[1 + \frac{3}{2}\frac{T_{\mathrm{rg}}}{T_{\mathrm{gr}}} + \frac{1}{2}\frac{T_{\mathrm{rg}}^2}{T_{\mathrm{gr}}^2}\right] + \frac{1}{2}\left[b_{\mathrm{er}}(1 + \frac{T_{\mathrm{rg}}}{T_1}) - b_{\mathrm{eg}}\frac{T_{\mathrm{rg}}}{T_{\mathrm{gr}}}\right]}{\left(1 + \frac{T_{\mathrm{rg}}}{T_{\mathrm{gr}}}\right)\left(2 + \frac{T_{\mathrm{rg}}}{T_{\mathrm{gr}}} + \frac{b_{\mathrm{er}}T_{\mathrm{rg}}}{T_1}\right)}. \qquad (27)$$

The first-order drift contribution to $\alpha_{\mathrm{R}}(\Delta_0)$ is zero by symmetry.

2.4.2. Error signal from drift

Expression (27) may look a little complicated, but all we really need to understand is the factor to the left of the $\times$-sign. This factor says, that α_{I} should be calculated by taking the background α_0 times "how far we climbed up the hole" (this is $\xi = \frac{\beta T_{\mathrm{rg}}}{\Gamma_{\mathrm{hole}}}$) times the relative depth, d_{hole}, of the hole. The rightmost fraction in Eq. (27) is merely a constant independent of laser power. Hence, this constant is the same for the center and side holes. In the, not so uncommon, case when $b_{\mathrm{er}}T_{\mathrm{rg}} \gg T_1$ (leading to $R \gg 1$) the factor is approximately equal to $[2(1 + \frac{T_{\mathrm{rg}}}{T_{\mathrm{gr}}})]^{-1}$. For brevity we make this approximation below. In the Pound-Drever-Hall scheme, the measured power on a photo-detector oscillating at ω_{m} becomes:

$$P_{\omega_{\mathrm{m}}}^{(\mathrm{out})}(t) = -P^{(\mathrm{in})}J_0J_1\alpha_0 L e^{-\frac{\alpha_0 L}{2}\left(\frac{\Gamma_{\mathrm{h}}}{\Gamma_{\mathrm{hole,c}}} + \frac{\Gamma_{\mathrm{h}}}{\Gamma_{\mathrm{hole,s}}}\right)} \frac{\beta T_{\mathrm{rg}}}{1 + \frac{T_{\mathrm{rg}}}{T_{\mathrm{gr}}}}\left[\frac{d_{\mathrm{hole,c}}}{\Gamma_{\mathrm{hole,c}}} - \frac{d_{\mathrm{hole,s}}}{\Gamma_{\mathrm{hole,s}}}\right]\sin(\omega_{\mathrm{m}}t). \qquad (28)$$

Comparing this expression to the low-frequency version in Eq. (24) we find most importantly that the difference in f-functions has been replaced by the difference in the ratios $d_{\mathrm{hole},i}/\Gamma_{\mathrm{hole},i}$. As discussed previously, there is a risk of obtaining the wrong sign for the error signal. The difference in square brackets in Eq. (28) must be positive for zero drift with $\beta = 0$ to be a stable solution. If this is not the case, there will be a bi-stable solution with positive or negative non-zero values of β. Since a particular value of β will give zero error signal, the frequency drift must be linear.

#83390 - $15.00 USD Received 25 May 2007; revised 17 Aug 2007; accepted 19 Aug 2007; published 24 Aug 2007

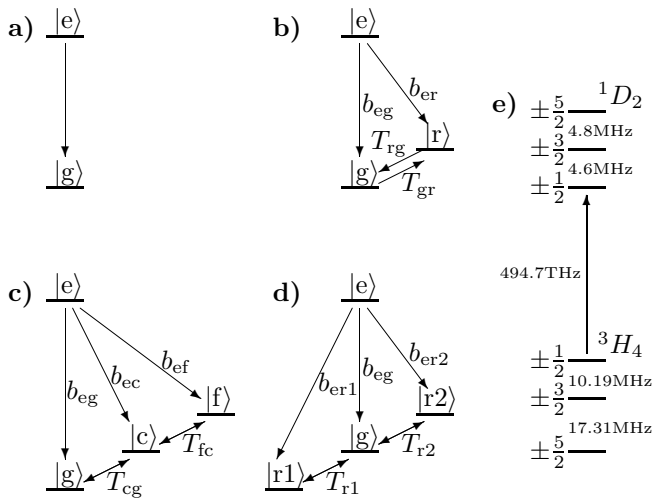

Fig. 4. Different level schemes used in this paper. We define timescales for relaxation between ground state levels and branching ratios from the excited state. The excited state lifetime is always denoted T_1. **(a)** The most naive scenario with two levels, considered in Sec. 2.1 and in the first row of Tab. 1. **(b)** Our basic model for all calculations, described in Secs. 2.2 and 2.4. Rows two to four in Tab. 1 refer to this case. Note, we may have different relaxation timescales $T_{\rm rg} \neq T_{\rm gr}$. **(c)** and **(d)** Different schemes with three ground states coupled as shown with RF-magnetic fields. Hence the timescale is the same in two opposite directions. These cases are reflected by rows five and six in Tab. 1, respectively. **(e)** The real Pr^{3+}:Y_2SiO_5 level scheme.

We wish to operate the laser stabilization system without this inherent linear drift, and to this end we derive a stability criterion based on convenient experimental parameters. The interplay between the carrier and sideband holes depends on the saturation parameter, m, and the actual strength of the hole-burning process, which can be parametrized by e.g. the measured carrier hole depth, $d_{\rm hole,c}^{\rm (meas)}$. The condition for the square brackets of Eqs. (24) and (28) to be positive, which is required for stability, is shown in Fig. 3.

Note, that it is easier to fulfill the criterion for correct low-frequency behavior than the criterion for no inherent linear drift. This is an important observation which shows that all the calculations regarding the drift model are worthwhile and necessary to obtain a complete understanding of laser stability. It is indeed possible that $d_{\rm hole,c}^{\rm (meas)}$ is in between the dotted and solid lines in Fig. 3, in which case the laser stabilization system is apparently locked but still the laser is drifting linearly. We also wish to note that the ratio, $d_{{\rm hole},i}/\Gamma_{{\rm hole},i}$, and the f-function describe, respectively, approximately and accurately the slope of the phase shift versus frequency when light passes the spectral hole. Hence, the physical origin (the interplay between the carrier and sidebands) of the two criteria shown in Fig. 3 is similar, whereas the actual difference is more of mathematical nature.

We conclude this section by pointing out that the drift calculations can be performed in a similar manner for a simple two-level system in absence of a reservoir state $|{\rm r}\rangle$, but the results can readily be guessed by setting $T_{\rm rg} = 0$, $T_{\rm gr} = \infty$, $b_{\rm er} = 1$, and $b_{\rm eg} = 0$. Then the three-level case will reduce to the two-level case and Eq. (27) will reduce to $\alpha_{\rm I}(\Delta_0) = -\frac{\alpha_0}{2}\frac{\beta T_1}{\Gamma_{\rm hole}} d_{\rm hole}$.

#83390 - $15.00 USD Received 25 May 2007; revised 17 Aug 2007; accepted 19 Aug 2007; published 24 Aug 2007

Table 1. The value of G and R for the different setups shown in Fig. 4. The first row gives the relations for the two-level atom (Fig. 4(a)) and the second row describes the two-level plus reservoir state system considered in Sec. 2.2 (Fig. 4(b)). The third and fourth rows are special cases of the second row. In the third row we assume $T_{gr} = \infty$, which describes a one-way natural decay from states $|r\rangle$ to $|g\rangle$. In the fourth row we assume $T_{rg} = T_{gr}$ which describes the case when an RF magnetic field couples the otherwise uncoupled states $|r\rangle$ and $|g\rangle$. The fifth and sixth rows correspond to the cases shown in Fig. 4(c) and Fig. 4(d), respectively, where there are two reservoir states. These four-level cases are presented since they resemble our experimental case using Pr^{3+}:Y_2SiO_5 as the atomic medium.

Case	G	R
Two-level	$G = 1$	$R = 1$
Three-level	$G = \frac{1}{1+\frac{T_{rg}}{T_{gr}}}$	$R = \frac{1+\frac{b_{er}T_{rg}}{T_1}}{1+\frac{T_{rg}}{T_{gr}}}$
Three-level, natural decay	$G = 1$	$R = 1 + \frac{b_{er}T_{rg}}{T_1}$
Three-level, RF eraser	$G = \frac{1}{2}$	$R = \frac{1}{2}[1 + \frac{b_{er}T_{rg}}{T_1}]$
Four-level, RF eraser (1)	$G = \frac{1}{3}$	$R = \frac{1}{3}[1 + \frac{2b_{ec}T_{cg}+b_{ef}(2T_{cg}+T_{fc})}{T_1}]$
Four-level, RF eraser (2)	$G = \frac{1}{3}$	$R = \frac{1}{3}[1 + \frac{T_{r1}b_{er1}+T_{r2}b_{er2}}{T_1}]$

2.5. General remarks on the calculations

Up until now we have considered a two-level system with a single reservoir state to model the trapping of atoms in the hole-burning process. This is a simple system which allows for not too complicated analytical solutions, thereby maintaining the physical understanding. This simple system is actually found in Tm^{3+}:$Y_3Al_5O_{12}$ [4, 10], and the even simpler pure two-level system is found in Er^{3+}:Y_2SiO_5 [7, 8] and Er:KTP [6].

However, more complicated cases exist. For our experiments with Pr^{3+}:Y_2SiO_5 there are three ground state levels and three excited state levels, see Fig. 4(e). In order to be able to estimate whether our experimental case resembles the simpler three-level system, we calculate $g(\Delta)$ for the more complicated case with three distinct ground states shown in Fig. 4(c,d). The active optical transition is still $|g\rangle \rightarrow |e\rangle$, but two reservoir states are present. In Fig. 4(c) the reservoir states are labeled $|c\rangle$ and $|f\rangle$ for "close" and "far", respectively, describing their position relative to the state $|g\rangle$. In Fig. 4(d) the symmetric case is shown with reservoir states $|r1\rangle$ and $|r2\rangle$. This distribution function, $g(\Delta)$, is found to have exactly the same form as Eq. (12), apart from new values of R and G, which are given in Tab. 1 (fifth and sixth rows).

We see that adding more ground reservoir states only changes the spectral holes quantitatively, but qualitatively we still have a Lorentzian-shaped hole fulfilling Eq. (12), as for the simple case of two-levels plus a single reservoir state. However, when all the nine transitions of Fig. 4(e) play the role of $|g\rangle \rightarrow |e\rangle$ due to the inhomogeneous broadening, the total distribution function, $g(\Delta)$, will in general be non-Lorentzian. We try in the experiments to keep this effect small, in order to mimic the three-level system and demonstrate the qualitative features of the theoretical calculations. The results in Tab. 1 will help us do this.

We also wish to remind the reader that our theory generally assumes perfect lasers or perfect lasers with harmonic errors. In practice, this is not the case, but our approximations are still quite good if the stabilization system maintains a narrow line-width. If the laser line width is e.g. 1 kHz and the hole width is 20 kHz, there will be some kind of folding effect of the

#83390 - $15.00 USD Received 25 May 2007; revised 17 Aug 2007; accepted 19 Aug 2007; published 24 Aug 2007

order of 5%. Also, we have assumed that $\alpha_0 L$ is not too large. If we, for example, set $\alpha_0 L \approx 1$ and assume a measured hole depth of around 50%, the transmission of the carrier beam is $e^{-1/2} \approx 60\%$. This means that the saturation parameter varies by 40% over the sample, and we can approximately take this into account by lowering the saturation parameter to 80% of the calculated value. In this manner (for the two levels plus a single reservoir state) we should be able to keep the theory quantitatively correct within around 10%, while all the qualitative features should hold true.

Finally, in our theoretical derivations of the error signal, we assumed the inhomogeneous profile of the transition to be infinitely broad with the consequence that the absorption of the modulation sidebands became identical. Relaxing this condition leads to another term in the error signal oscillating as $\cos(\omega_m t)$ and essentially being proportional to the derivative of the inhomogeneous absorption profile versus frequency [23]. This effect can be utilized as a fixed frequency reference for the laser stabilization [4, 24].

3. Experimental setup

We have stabilized a Coherent CR699-21 dye laser to the 606 nm transition in Pr^{3+}:Y_2SiO_5. The theoretical calculations of Sec. 2 assisted us in choosing the optimum parameters of the electronic feedback system for best performance. It is not the purpose of this paper to describe the electronic system, which consists of standard techniques. However, for completeness we mention a few design considerations below. For further details we refer to [25, 26].

The main building blocks of the laser stabilization system are shown in Fig. 5. In the upper right corner we show the commercial version of the dye laser, where we placed an intra-cavity electro-optical modulator (EOM 1). We fed the two electrodes by two separate amplifier circuits, IC1 and IC2.

From the laser output the laser beam was directed through another electro-optical modulator (EOM 2) applying $\omega_m = 2\pi \cdot 50$ MHz modulation from a local oscillator. The modulated beam was then expanded to cover the entire area of a Pr^{3+}:Y_2SiO_5 crystal with diameter of 19 mm, thickness of 5 mm, and doping concentration 0.005%, kept in a cryostat operated at 3.0 K. The peak absorption of the inhomogeneous profile is $\alpha_0 L = 1.9$ corresponding to a transmission of $e^{-\alpha_0 L} \approx 15\%$.

Surrounding the crystal are two sets of coils allowing us to couple RF-magnetic fields to the 10.19 MHz and the 17.31 MHz hyperfine level transitions. The RF fields are generated as sawtooth sweeps, the 10.19 MHz signal is 100 kHz wide, and the 17.31 MHz signal is 200 kHz wide. The sweep time is 0.82 ms, which is comparable to the hyperfine level coherence time of 0.50 ms and hence the pumping becomes effectively incoherent. This procedure assures smooth re-population over time of the hyperfine levels since atoms with different frequencies on the inhomogeneous hyperfine transition are affected at different times.

After the light has passed the crystal it is detected and demodulated at the frequency ω_m and filtered to give the error signal. Based on this, the laser frequency is actuated using EOM 1 which is driven by the analog electronics shown in Fig. 5(a) around IC1 and IC2. The complex electronic gain from the error signal to the voltage across the electrodes of EOM 1 is given by:

$$g(\omega) = \frac{R_2}{R_1} \cdot \frac{i\omega(R_3+R_4)C+1}{i\omega R_3 C}. \tag{29}$$

We see that there is a characteristic cutoff frequency, $f_c = \frac{\omega_c}{2\pi} = \frac{1}{2\pi(R_3+R_4)C}$, which separates this gain into a low-frequency part proportional to $\frac{1}{i\omega}$ and a high-frequency part where the gain is constant and real. We choose the component values such that the critical frequency, ω_c, is close to Γ_{hole}. In this manner the electronic gain of Eq. (29) together with the medium- and high-

#83390 - $15.00 USD Received 25 May 2007; revised 17 Aug 2007; accepted 19 Aug 2007; published 24 Aug 2007

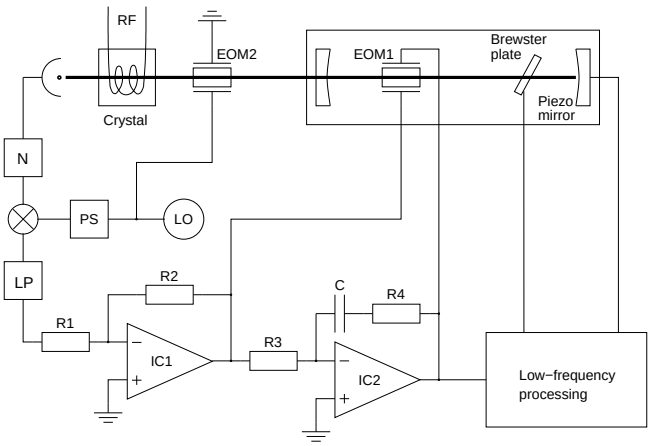

Fig. 5. Optical and electronic design schematics. Abbreviations: N, notch filter; LP, low-pass diplexer; PS, phase shifter; LO, local oscillator; EOM, electro-optical modulator. See the text for more details.

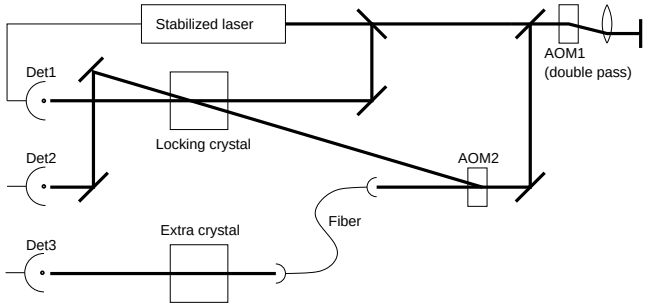

Fig. 6. Experimental setup for characterizing the spectral hole dynamics. Apart from the locking beam needed for the laser stabilization system, we place an additional probing beam for characterizing the dynamics of the locking itself. AOM 1 is in double pass configuration and allows us to scan the laser beam frequency without any beam motion. AOM 2 allows us to shift back to the original stabilized laser frequency to characterize the holes when the laser is locked. An extra crystal in another cryostat is used for measuring the laser frequency drift on long timescales.

frequency part of the atomic response shown in Fig. 2(a) add up to a total response proportional to $\frac{1}{i\omega}$.

The output of IC2 was also sent to a low-frequency, digital proportional-integral (PI) regulator, i.e. an amplifier with gain $g(\omega) \propto \frac{c_1}{i\omega} + c_2 \propto \frac{1/\tau + i\omega}{i\omega}$. We chose τ to be equal to a typical value for the hole lifetime, T_{rg}, matching the low- to medium-frequency response of Fig. 2(a). The output was sent into the commercial parts of the laser control adjusting the Brewster plate and the piezo-mounted mirror. In this manner, the total response of the atomic medium and our electronic system at all frequencies becomes proportional to $\frac{1}{i\omega}$. This is known from feedback theory [27] to assure stable operation.

For our study of the hole-burning dynamics, we have in addition to the stabilization setup of Fig. 5 constructed the optical setup shown in Fig. 6. The combination of AOMs 1 and 2 allow us to measure simultaneously the shape of the carrier and sideband holes using the coherent readout technique described in [28, 29]. Examples of hole shapes are given in Fig. 8(a,b). These

#83390 - $15.00 USD Received 25 May 2007; revised 17 Aug 2007; accepted 19 Aug 2007; published 24 Aug 2007

shapes can be correlated to the laser drift, which can be measured by burning a spectral hole in an auxiliary crystal and measuring its position over time, see Fig. 7 for an example.

4. Experimental results

In this section we wish to present some experimental verification of the theory concerning the drift dynamics in Sec. 2.4. In particular, in Sec. 4.2 we will study the correlations between the hole shapes and the laser drift, and we will test the drift criterion of Fig. 3. We will also comment briefly on the short time stability of the laser in Sec. 4.3, but before that we will in Sec. 4.1 compare our particular system using Pr^{3+}:Y_2SiO_5 to the theoretical models of Sec. 2. We conclude the experimental section with a discussion of our results.

4.1. Comparing Pr^{3+}:Y_2SiO_5 to the theoretical model

As shown in Fig. 4(e), there are three ground and three excited states in Pr^{3+}:Y_2SiO_5. The transition strengths between these are very different; the strongest are $\pm\frac{1}{2} \rightarrow \pm\frac{1}{2}$ (0.55), $\pm\frac{1}{2} \rightarrow \pm\frac{3}{2}$ (0.38), $\pm\frac{3}{2} \rightarrow \pm\frac{1}{2}$ (0.40), $\pm\frac{3}{2} \rightarrow \pm\frac{3}{2}$ (0.60), and $\pm\frac{5}{2} \rightarrow \pm\frac{5}{2}$ (0.93), while the remaining four are weak (0.07 or less) and have smaller influence on the locking. The numbers in parentheses are the relative strengths taken from [30] and we assume that these are also valid for branching ratios in the decay process. We see that the ions typically stay within the $\pm\frac{1}{2}, \pm\frac{3}{2}$ space or in the $\pm\frac{5}{2}$ state, and only seldom change between these (the total crossing probability being 7%). If this crossing occurs, the RF pumping on the ground state hyperfine transition $\pm\frac{5}{2} \rightarrow \pm\frac{3}{2}$ at 17.31 MHz transition will counteract it. Since the crossing is infrequent, the timescale for this RF transition $T_{17\mathrm{MHz}}$ can be relatively slow (in order to maintain a certain hole depth). On the other hand, an ion resonant on, e.g., the $\pm\frac{1}{2} \rightarrow \pm\frac{1}{2}$ optical transition will decay to the ground $\pm\frac{3}{2}$ state with a high probability (40%), and the RF pumping on the hyperfine transition $\pm\frac{3}{2} \rightarrow \pm\frac{1}{2}$ at 10.19 MHz must counteract this with a relatively short timescale $T_{10\mathrm{MHz}}$ (to maintain the same hole depth for this atomic species). In all experiments (apart from some of those illustrated in Fig. 8) we have set $T_{17\mathrm{MHz}} = 10 \cdot T_{10\mathrm{MHz}}$. Hence, by combining a small branching ratio for the optical decay taking an atom away from the resonant transition with a long timescale for the RF pumping bringing the atom back to the resonant transition (or vice versa), we ascertain that the parameter R is similar for the atomic species resonant on the five transitions mentioned above (according to the results in Tab. 1). Since, also, the strengths of these five transitions are not that different, we expect to see experimental results not too different from the simple three-level model of Fig. 4(b).

4.2. Laser drift dynamics

Let us now turn to the experimental results concerning the laser drift and the hole shapes in the locking crystal. A direct evidence of linear frequency drift of the laser is shown in Fig. 7(a), and in the following we will connect the observation of laser drift to the hole shapes.

In Sec. 2.4 we argued that if the spectral holes used for locking are too deep, the laser may be locked but drifting linearly in frequency, which in turn will cause the hole shape to be asymmetric. Such asymmetry is demonstrated in Fig. 8(a,b), showing in each color pairs of shapes for the carrier and sideband holes. From the measured hole shape, $\alpha_{\mathrm{R}}(\omega)L$, we can calculate the imaginary part, $\alpha_{\mathrm{I}}(\omega)L$, by using the Kramers-Krönig relations [31]. In our case, the Kramers-Krönig relations take a slightly simpler form than usual since the only ω-dependence in Eq. (4)

#83390 - $15.00 USD Received 25 May 2007; revised 17 Aug 2007; accepted 19 Aug 2007; published 24 Aug 2007

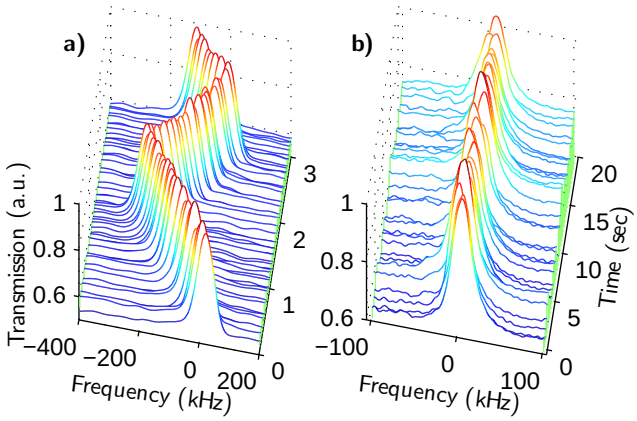

Fig. 7. (Color online) Example of drift measurements. **a)** Total observation time is 3 seconds and we see a drift rate of roughly 160 kHz/s, where the direction changes occasionally. **b)** Total observation time is 20 s and the drift is 0.3 kHz/s over this time.

is in the denominator $\frac{\Gamma_h}{2} + i(\Delta - \omega)$. It can be shown that:

$$\begin{aligned} \alpha_R(\omega_0) &= +\lim_{\delta\to 0}\frac{1}{\pi}\int_{-\infty}^{\infty}\frac{\alpha_I(\omega)(\omega-\omega_0)d\omega}{(\omega-\omega_0)^2+\delta^2}, \\ \alpha_I(\omega_0) &= -\lim_{\delta\to 0}\frac{1}{\pi}\int_{-\infty}^{\infty}\frac{\alpha_R(\omega)(\omega-\omega_0)d\omega}{(\omega-\omega_0)^2+\delta^2}. \end{aligned} \tag{30}$$

Since $\alpha_I(\omega_0)$ is an integral of $\alpha_R(\omega)$ times an odd function in $\omega - \omega_0$, the value of $\alpha_I(\Delta_0)$ directly measures the hole asymmetry. In Fig. 8(c) we compare this measure for the center and side hole shapes. The data points are taken for a number of different settings of $T_{10\mathrm{MHz}}$ and $T_{17\mathrm{MHz}}$. We see a clear proportionality, $\alpha_I^{(\mathrm{side})}(\Delta_0) = 0.72 \cdot \alpha_I^{(\mathrm{carrier})}(\Delta_0)$.

We expect $\alpha_I^{(\mathrm{carrier})}(\Delta_0)$ and $\alpha_I^{(\mathrm{side})}(\Delta_0)$ to be equal, since from Eq. (6) the phase shifts, of the carrier ϕ_c and sideband ϕ_s are proportional to $\alpha_I^{(\mathrm{carrier})}(\Delta_0)$ and $\alpha_I^{(\mathrm{side})}(\Delta_0)$, respectively, and with a closed laser stabilization feedback loop we must have zero error signal with $\phi_c = \phi_s$. The reason for the slope not being unity is unknown.

The direct observations of the drift, as exemplified in Fig. 7(a), the proportionality in Fig. 8(c), and the fact that the electronic error signal is small shows that the laser may drift linearly, while the feedback loop is still locked.

The hole asymmetry is correlated to the laser drift rate. The detailed understanding of this correlation requires a complete solution of the equations of motion discussed in Sec. 2.4 and is outside the scope of this paper. Instead, in the following we will examine the measured drift rate, β, for various parameter settings. The results of these measurements are shown in Fig. 9. The light intensity is kept constant with the saturation parameter $s_0 \approx 0.09$. The modulation index, m, has the values 0.14, 0.20, 0.28, 0.40, and 0.56, and each color in Fig. 9 corresponds to one of these values. The hole shapes are controlled by employing $T_{10\mathrm{MHz}} = \frac{1}{10} \cdot T_{17\mathrm{MHz}}$ at the six values 2 ms, 4 ms, 8 ms, 20 ms, 40 ms, and 80 ms. In Fig. 9 the six corresponding data points are plotted for each color from left to right since the hole depth $d_{\mathrm{hole,c}}^{(\mathrm{meas})}$ increases with $T_{10\mathrm{MHz}}$.

We have obtained low drift rates in the left part of the Fig. 9 (the lowest measured being below 0.5 kHz/s). However, the drift rates increase when the hole depth increases. In order to

#83390 - $15.00 USD Received 25 May 2007; revised 17 Aug 2007; accepted 19 Aug 2007; published 24 Aug 2007

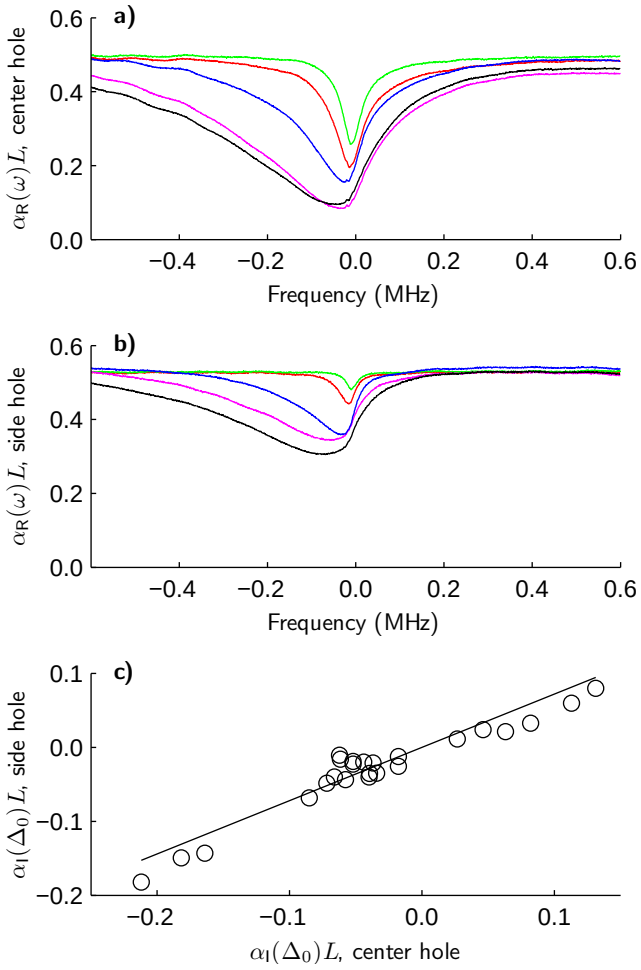

Fig. 8. (Color online) In the two upper graphs the measured absorption, $\alpha_R(\omega)L$, is plotted for comparison under different conditions for a number of center holes **(a)** and side holes **(b)**. With increasing hole depth, the asymmetry of both increases. The imaginary part, $\alpha_I(\Delta_0)$, of the absorption coefficient at the hole center is a quantitative measure of this asymmetry, and can be calculated from $\alpha_R(\omega)$ using the Kramers-Krönig relations (30). In **(c)** we see, for several measurements under different conditions, a clear linear relationship between this asymmetry for the center and side holes. The straight line is a fit through the origin with a slope of 0.72, theoretically we expect a slope of unity.

obtain these data, we had to carefully adjust the phase of the demodulation of the error signal while observing the drift rate decreasing for one of the parameter settings in the left-side of 9. This is a consequence of the fact that the transient spectral hole is not a fixed frequency reference, and if there is an offset in the feedback system, the locking point would be slightly off-center in the hole leading to a frequency drift. We placed the laser frequency on the side of the inhomogeneous profile in order to decrease $\alpha_0 L$ from the peak value of 1.9 to a more moderate and useful value of 0.66 corresponding to $e^{-\alpha_0 L} \approx 0.5$. Hence, being away from the inhomogeneous profile center, we expect small corrections to the calculated error signal Eq. (23) since the phase shift from the background inhomogeneous profile plays a minor role

#83390 - $15.00 USD Received 25 May 2007; revised 17 Aug 2007; accepted 19 Aug 2007; published 24 Aug 2007

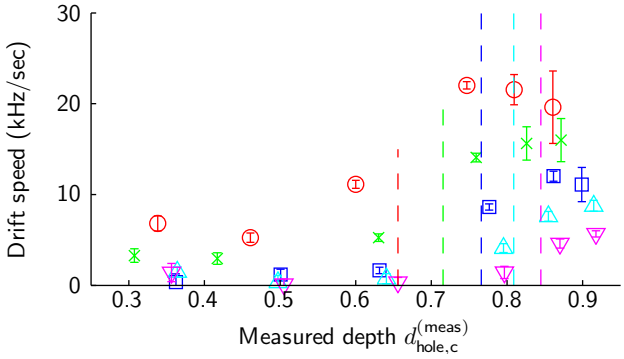

Fig. 9. (Color online) Measured drift rates versus measured hole depth. The hole shapes are changed by varying $T_{10\text{MHz}}$ and $T_{17\text{MHz}}$. Red circles, $m = 0.56$; green crosses, $m = 0.40$; blue squares, $m = 0.28$; cyan triangles up, $m = 0.20$, purple triangles down, $m = 0.14$. The vertical dashed lines indicate the values of the corresponding thresholds shown in Fig. 3.

(see the approximation of Eq. (19)). Also, a small error in the phase setting would mix in a part of the $\cos(\omega_{\text{m}}t)$ quadrature, which is also dependent on the inhomogeneous absorption profile. The joint effect of these corrections is effectively a small offset, but the small phase adjustments counteracted this.

However, the drift rates on the right-hand side of Fig. 9 did not decrease in this fine-tuning procedure. A slight change in error signal offset cannot change the fact that zero drift is an unstable solution if the criterion in Fig. 3 is not met. The vertical lines in Fig. 9 represent this threshold value for each modulation index, and the drift rates increase consistently for hole-depths above these values.

We have observed examples of much higher drift rates than 25 kHz/s, see e.g. Fig. 7(a) where, in addition to a high drift rate of 160 kHz/s, we also saw that the direction changed occasionally. In this example, the drift rate is similar in both directions, which is consistent with a bi-stable solution to the equations of motion with inherent linear frequency drift.

4.3. Laser phase stability

In the previous section we demonstrated that with the right parameter choice, the inherent linear frequency drift could be excluded leaving us with a low drift of the order of 1 kHz/sec limited by offset tolerances and possibly by detection noise. In this section we demonstrate that with the same parameters the short term phase stability can also be satisfactory.

In the experiment we modified the setup shown in Fig. 6 slightly such that the zeroth-order diffracted beam from AOM 2 (which is not turned on) is sent to the locking crystal. AOM 1 is operated around its 200 MHz center frequency and hence, with the frequency shifted around 400 MHz in double pass configuration, the probing beam will not interfere with the laser locking system.

We used optical FID to measure the laser stability and to this end we programmed the pulse sequence shown in Fig. 10(a). The laser is scanned back and forth during pulse “1” within a 10 MHz interval removing all ions herein by optical pumping. The frequency of pulse “4” is then later chosen such that it falls within this interval, which is empty of absorbing ions. In this way pulse “4” does not induce any polarization on its own. When pulse “2” is applied a coherence is set up in the atomic medium and when pulse “2” is turned off the atoms will keep radiating for a time limited by the optical coherence time, T_2, (which in our case is around 18 μs) and also by

#83390 - $15.00 USD Received 25 May 2007; revised 17 Aug 2007; accepted 19 Aug 2007; published 24 Aug 2007

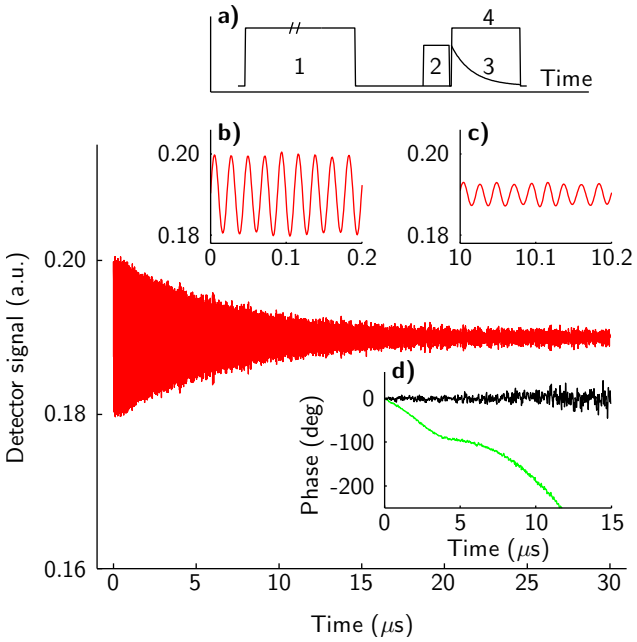

Fig. 10. (Color online) Illustration of the phase stability measurements. Inset **a)** shows the pulse sequence for the experiment: (1) is a 10 ms burn pulse scanning between 40 MHz and 50 MHz (relative to the AOM double-pass center). After waiting 100 μs, pulse (2) with a constant frequency of zero and duration 40 μs sets up a coherence in the atoms which leads to the FID at (3). Finally, pulse (4) at a frequency of 45 MHz beats with the FID, leading to the detector signal shown (after filtering) in the main panel. The traces in insets **b)** and **c)** show this signal in a 200 ns window around time 0 and 10 μs, respectively, and the phase of these oscillations can be calculated with a good signal-to-noise ratio. Inset **d)** shows the calculated phase as a function of time for the stabilized (black) and unstabilized (green) laser.

the inverse bandwidth of the actual coherence. This decaying radiation "3" gives a fingerprint of the phase of the laser during pulse "2". At the same time, we apply another pulse, "4", shifted 45 MHz in frequency carrying its own phase. The beating of pulses "3" and "4" hence compares the present phase and the past phase, and comparing the measured oscillations with a 45 MHz local oscillator allows us to calculate the short term characteristics of the laser.

The data in Fig. 10 is obtained with $T_{10\mathrm{MHz}} = \frac{1}{10} \cdot T_{17\mathrm{MHz}} = 4$ ms, modulation index $m = 0.20$, and saturation parameter $s_0 \approx 0.09$. These settings is represented in Fig. 9(c) giving a drift of (0.34 ± 0.76) kHz/s. Performing the experiment of Fig. 10 several times allows us to determine the statistics of the phase fluctuations. On the 10 μs timescale the laser phase standard deviation is below 4 degrees corresponding to a linewidth of approximately 1 kHz. We conclude that a slow frequency drift rate can be obtained together with a high phase stability.

4.4. Discussion of the results

Let us briefly summarize the experimental results. Our main objective of the experimental part of this paper is to study the hole-burning dynamics in connection with laser frequency drift. We have demonstrated that the asymmetry of the spectral hole increases with increasing hole depth, and for holes deeper than the threshold of Fig. 3 an increased drift rate has been observed. Also, the direct observation of a bi-stable drift underlines the interpretation that a linear laser

#83390 - $15.00 USD Received 25 May 2007; revised 17 Aug 2007; accepted 19 Aug 2007; published 24 Aug 2007

frequency drift can be an inherent solution to the equations of motion, even though the feedback loop is closed and the error signal is small. The calculated threshold values for this inherent linear drift are consistent with our observations. Adjusting the experimental parameters, we were able to obtain a linear frequency drift rate below 1 kHz/sec, and for these parameters we also demonstrated a short term stability corresponding to a linewidth of 1 kHz on 10 μs timescales.

We also wish to note that we have considered different experimental parameter settings. In general, the best phase stability performance is found for the parameters of the example in Sec. 4.3. Together with our chosen optical power these parameters give rise to a measured hole depth, $d_{\mathrm{hole,c}}^{(\mathrm{meas})}$, around 0.5 to 0.6 in Fig. 9. This value for the hole depth gives a large error signal (corresponds to $x = \frac{\Gamma_{\mathrm{hole}}}{\Gamma_{\mathrm{h}}} \approx 2$, which is essentially the optimum choice according to the f-function Eq. (25) shown in Fig. 1). We have also investigated a few different positions on the inhomogeneous profile. These measurements indicate that a transmission above 30% is a good choice, which is also consistent with theoretical expectations. We conclude that in general the stabilized laser performs very well with settings close to the optimum values discussed in Sec. 2.3.2.

Laser stabilization using a spectral hole or the inhomogeneous profile has been reported previously for semiconductor lasers in several publications [5, 6, 4, 7, 8, 3, 9, 24]. Compared to the results herein, our stabilized laser performs very well for short timescales, whereas much slower drift rates have been reported on long timescales than our value of 1 kHz/sec. The reason for the latter is the fact that we did not incorporate the inhomogeneous profile as a fixed frequency reference, but this is straightforward to do, see e.g. [4]. To improve stability, we believe that the threshold condition for inherent laser drift is also important in cases where the inhomogeneous profile is included as a fixed frequency reference.

5. Conclusion

By introducing an analytical theory, we have contributed to the understanding of laser stabilization using spectral holes to an extent that we hope will enable other scientists to further improve existing technology. In particular, we calculated a transfer function describing the atomic response to errors in the laser frequency, and we have identified a solution to the equations of motion with an inherent linear frequency drift of the stabilized laser. We have provided experimental support for the part of the theory concerning the laser drift, and our general experience tell us that the optimum parameters suggested by theory also gives the best performance in practice.

Acknowledgments

We are grateful to Mike Jefferson and Pete Sellin for sharing their detailed knowledge on laser stabilization. We also wish to thank Krishna Rupavatharam for introducing the coherent readout technique. This work was supported by the European Commission through the ESQUIRE project and the integrated project QAP under the IST directorate, by the Knut and Alice Wallenberg Foundation, and the Swedish Research Council. B. Julsgaard is partly supported by the Carlsberg Foundation.

#83390 - $15.00 USD Received 25 May 2007; revised 17 Aug 2007; accepted 19 Aug 2007; published 24 Aug 2007